

# Selective hydrogenation of bio-based 5-hydroxymethyl furfural to 2,5-dimethylfuran over magnetically separable Fe-Pd/C bimetallic nanocatalyst

Abhijit D. Talpade, Manishkumar S. Tiwari, Ganapati D. Yadav\*

Department of Chemical Engineering, Institute of Chemical Technology, Nathalal Parekh Marg, Matunga, Mumbai, 400 019, India

## ARTICLE INFO

### Keywords:

2,5-Dimethylfuran  
5-Hydroxymethyl furfural (HMF)  
Fe-Pd/C  
Bimetallic catalyst  
Selective hydrogenation  
Green chemistry

## ABSTRACT

There is an ever increasing need to innovate and provide alternative energy sources to reduce the over-dependence on conventional fossil fuels. 2, 5-Dimethylfuran (DMF), a bio-based chemical, has gained a lot of attention due to its potential application as a biofuel additive and is synthesized through hydrogenation of 5-hydroxymethylfurfural (HMF). Bimetallic nano-catalysts have gained importance in recent years due to their excellent selectivity and activity. In this paper, a magnetically separable Fe-Pd/C bimetallic nano-catalyst was developed which not only showed excellent selectivity to DMF but also helped reduce the noble metal consumption, thereby making the catalyst cheaper. Using XPS, XRD and TPR characterization techniques, the Fe-Pd/C catalyst was found to exist as bimetallic containing a partially oxidized Fe and reduced Pd atoms. It exhibited 85% selectivity towards DMF with 100% conversion of HMF. The reaction was conducted in a liquid-acid-free environment, thus making the process environmental friendly. The oxidized Fe imparts magnetic properties to the catalyst making it easy to recover. The catalyst was found to be robust and showed excellent activity on repeated use. Overall a highly efficient, economic and green process for DMF synthesis was developed based on biomass as feedstock.

## Introduction

There is an increasing demand for alternative energy sources due to the ongoing issues like global warming and reduction in reserves of conventional fossil fuels. Biofuels have emerged as an option to these problems. Biofuel additives such as furanic ethers and esters, or 2,5-dimethylfuran can be derived from simple processes like condensation and hydrogenation of 5-hydroxymethylfurfural (HMF), which could be derived from various simple and complex sugars like glucose, fructose, etc. [1–3].

The presence of two functional groups in the furan ring of HMF molecule provides an opportunity of converting it into various value-added chemicals that find applications in various fields [4,5]. The products obtained by hydrogenation of HMF typically are 2,5-dihydroxymethyl furan (DHMF), 2, 5-dimethylfuran (DMF), and ring-opened products [6,7]. Scheme 1 gives the reaction products of hydrogenation of HMF.

Of all these products, 2, 5-dimethylfuran (DMF) is more promising due to its superior properties such as ideal boiling point (92–94 °C), high energy density (30 kJ cm<sup>-3</sup>), and high research octane number (RON = 119). Furthermore, it blends easily with gasoline and is immiscible with water; and thus it proves to be a better additive than

ethanol which is miscible with water [8].

For synthesis of DMF by hydrogenation of HMF, hydrogen must react selectively with the formyl and hydroxyl groups attached to the furan ring and avoid excessive hydrogenation or ring-opening of the furanic molecule, as shown in Scheme 1, to prevent formation of additional by-products [9]. Thus, the main aim in the case of hydrogenation is to control the selectivity of the desired product using a highly active and selective catalyst. This can be achieved by maintaining optimum reaction conditions and by designing catalysts that show high selectivity. Commonly used catalysts for the conversion of HMF to DMF are CuRu/C and Pd/C. Román-Leshkov et al. [10] produced DMF from fructose using one-pot synthesis, wherein HMF was synthesized from fructose using an acid catalyst and then transformed it to DMF by using CuRu/C catalyst. The catalyst was found to deactivate and required regeneration. Also, the bimetallic CuRu/C catalyst was found to be affected to a certain extent by the chloride ions present in the system. A milder pathway to produce DMF in excellent yield was reported by employing an acidic reagent such as formic acid and Pd/C as catalyst [11]. However, there was a need to use corrosive formic acid and H<sub>2</sub>SO<sub>4</sub> to obtain high yields making it a polluting process. Chidambaram and Bell [12] produced DMF from glucose using a two-step reaction with an acidic catalyst for dehydration followed by a metallic

\* Corresponding author.

E-mail address: [gd.yadav@ictmumbai.edu.in](mailto:gd.yadav@ictmumbai.edu.in) (G.D. Yadav).

### Nomenclature

A	Reactant species A, 5-hydroxymethyl furfural (HMF)
S	Catalyst active site
AS	Chemisorbed species A
HS	Chemisorbed hydrogen (dissociative adsorption)
B	First intermediate product, 2,5- dihydroxymethyl furan (DHMF)
BS	Chemisorbed species B
W	Water
C	Second intermediate product, hydroxymethyl furan
CS	Chemisorbed species C
D	Final product, 2,5- dimethyl furan (DMF)
DS	Chemisorbed species D
C <sub>A</sub>	Concentration of A, (mol/L)
C <sub>AS</sub>	Concentration of A at solid (catalyst) surface, (mol/g-cat)
C <sub>H2</sub>	Concentration of hydrogen, (mol/L)
C <sub>HS</sub>	Concentration of hydrogen at solid (catalyst) surface, (mol/g-cat)
C <sub>B</sub>	Concentration of B, (mol/L)
C <sub>BS</sub>	Concentration of B at solid (catalyst) surface, (mol/g-cat)
C <sub>W</sub>	Concentration of water, (mol/L)
C <sub>C</sub>	Concentration of C in liquid phase (mol/L)
C <sub>CS</sub>	Concentration of C at solid (catalyst) surface, (mol/g-cat)
C <sub>D</sub>	Concentration of D in liquid phase, (mol/L)
C <sub>DS</sub>	Concentration of D at solid (catalyst) surface, (mol/g-cat)
C <sub>S</sub>	Concentration of vacant sites, (mol/g-cat)
C <sub>T</sub>	Total concentration of sites, (mol/g-cat)
r <sub>AD</sub>	Rate of chemisorption reaction of A (mol L <sup>-1</sup> min <sup>-1</sup> )

K <sub>A</sub>	Equilibrium constant for the adsorption reaction of A (L/mol)
r <sub>HD</sub>	Rate of chemisorption reaction of H (mol L <sup>-1</sup> min <sup>-1</sup> )
K <sub>H</sub>	Equilibrium constant for the adsorption reaction of H (L/mol)
k <sub>1</sub>	Reaction rate constant for forward reaction of A to B
k <sub>1</sub> '	Reaction rate constant for backward reaction of A to B
k <sub>2</sub>	Reaction rate constant for forward reaction of B to C
k <sub>2</sub> '	Reaction rate constant for backward reaction of B to C
k <sub>3</sub>	Reaction rate constant for forward reaction of C to D
k <sub>3</sub> '	Reaction rate constant for backward reaction of C to D
-r <sub>1</sub>	Rate of surface reaction 1, A to B (mol L <sup>-1</sup> min <sup>-1</sup> )
-r <sub>2</sub>	Rate of surface reaction 2, B to C (mol L <sup>-1</sup> min <sup>-1</sup> )
-r <sub>3</sub>	Rate of surface reaction 1, C to D (mol L <sup>-1</sup> min <sup>-1</sup> )
K <sub>1</sub>	equilibrium reaction constant for reaction 1, A to B, dimensionless
K <sub>2</sub>	Equilibrium reaction constant for reaction 2, B to C, dimensionless
-r <sub>D</sub>	Rate of desorption reaction of species D (mol L <sup>-1</sup> min <sup>-1</sup> )
K <sub>D</sub>	Equilibrium constant for the adsorption reaction of D (L/mol)
k''	Consolidated rate constant in Eq. (31) (L g-cat <sup>-1</sup> min <sup>-1</sup> )
S	Vacant active sites
w	Catalyst loading (g-cat/L)

### Acronyms

HMF	5-Hydroxymethylfurfural
DMF	2,5-Dimethylfuran

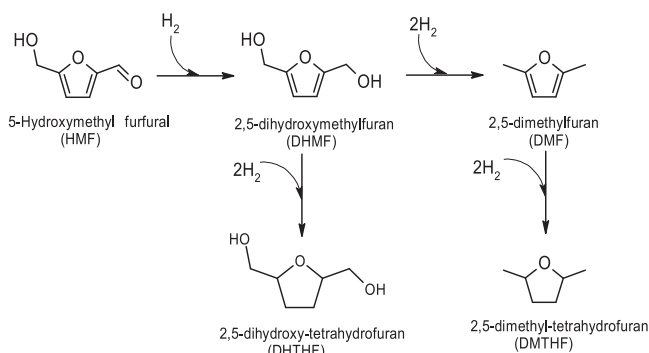
catalyst for HMF to DMF conversion. Maat et al. [13] studied the synthesis of DMF by combining Pd/C catalyst and HCl as an activator in alcohol as solvent. It is seen that most of the reports require use of an acid as a reagent to improve yields of DMF. Recent reports on carrying out the transformation of HMF to DMF using catalysts like Ru/Co<sub>3</sub>O<sub>4</sub> have yielded high yields of up to 94% while using mild conditions [8]. Current reports based on Ni catalysts have shown that high selectivity of DMF along with high HMF conversions can be achieved [14,15].

As given in Scheme 1, due to different functionalities in HMF molecule, an array of products can be formed during the process of hydrogenation leading to reduction in yields of DMF and thus increasing product purification costs. Exploration of bimetallic catalysts could be considered as one of the approaches for improved DMF yield. For example, Cu addition in bimetallic catalyst, CuRu/C, helps in improving the selectivity of DMF with 71% yield. These experiments were performed at 220 °C and 6.8 bar H<sub>2</sub> pressure [10]. Wang et al. have obtained 98% DMF yield at 180 °C and 10 bar hydrogen pressure using Pt-Co catalyst [16]. Nishimura et al. [17] have employed Pd-Au/C and HCl as catalyst at very moderate operating conditions (60 °C) and at

atmospheric hydrogen pressure and achieved exceptional yields of DMF. Recent reports involving bimetallic catalysts using cobalt as a metal have also shown promise [18,19].

Bimetallic systems help provide an added degree of freedom for tuning the catalytic performance by modifying the electronic and geometric structures of these materials which can be done by changing the composition and size of the materials used [16,20]. Bimetallic catalysts help in improving the selectivity, stability and activity as compared to monometallic counterparts and are active even under mild conditions [21–30]. Bimetallic nanomaterials are turning out to be the most promising catalysts due to their superior catalytic properties. As most of the catalytic reactions take place on the surface of nano-sized catalysts, their interior atoms are often rendered useless. This poses a serious problem when costly noble-metals such as Pd or Pt-based catalysts are used. The noble metals in the central core could be replaced by alloying with other transition metals like Cu, Fe, Co and Ni, which not only help reduce the catalyst cost but also show a marked improvement in the catalytic activities due to the synergistic effects resulting from geometric and electronic interactions of the two metals used [28,29]. Metals such as iron are available in abundance and show excellent magnetic properties. On successfully employing these metals in the catalyst, it is possible to obtain materials that are cheap to produce and easy to recover by using an external magnetic field, due to magnetic properties exhibited by them [28,31].

We report here the selective hydrogenation of 5-hydroxymethylfurfural (HMF) to 2,5-dimethylfuran (DMF) using magnetically separable bimetallic nano-catalysts synthesized using the sequential reduction method. Different bimetallic combinations have been tried by combining iron with other metals (like Pd, Cu) as it provides the additional advantage of easier separation using external magnetic field. Various parameters have been optimised to obtain maximum yield of DMF. The reaction mechanism and kinetics have been proposed. Unlike the usual processes, the process has been performed in an acid-free environment, thus making it greener. High yields



**Scheme 1.** Products from hydrogenation of HMF.

of DMF are obtained using bimetallic nano-catalysts which also show excellent reusability characteristics.

## Experimental

### Materials

Ferrous chloride anhydrous, cuprous chloride, activated charcoal pellets and sodium borohydride, n-butanol, n-decane and 5% w/w Pd/C, were procured from SD Fine Chemicals Limited, Mumbai, India. Palladium chloride was procured from Sigma Aldrich, Mumbai. Tetrahydrofuran and 1, 4-dioxane was procured from Thomas Baker, Mumbai. All these chemicals were of analytical grade and required no purification before their use. HMF used in the experiments was synthesized in the lab through a biphasic method developed in the laboratory. The purity assay of the HMF synthesized was studied using <sup>1</sup>H-NMR and was found to be 98% pure.

### Catalyst synthesis

#### Iron-palladium on carbon catalyst synthesis

Fe-Pd bimetallic catalyst, supported on carbon was synthesized using the sequential reduction process as described in prior art with a few modifications [28]. Firstly the activated charcoal (100 mg) was sonicated at room temperature in 30 mL water for 30 min for high dispersion of . To this mixture, excess NaBH<sub>4</sub> (676.2 mg) was added. For formation of Fe in the Fe-Pd bimetallic catalyst (molar ratio Pd:Fe = 1:20), 289.6 mg FeCl<sub>3</sub> was dispersed in 30 mL water and sonicated for 10 min. FeCl<sub>3</sub> solution was then added into the mixture drop-wise to bring about reduction of Fe from Fe<sup>3+</sup> to Fe<sup>0</sup>. The mixture was then agitated for 30 min to ensure complete release of hydrogen. PdCl<sub>2</sub> solution was prepared by taking 27 mg of PdCl<sub>2</sub> in 20 mL water. To aid the dissolution of PdCl<sub>2</sub> salt in water, small amount of NaCl (500 mg) was added. The prepared PdCl<sub>2</sub> solution was further added to Fe/C solution, drop-wise, and stirred for 1 h. It was found that some of the Fe atoms present on the outer-layer were sacrificed to bring about Pd reduction from Pd<sup>2+</sup> to Pd<sup>0</sup>. Bimetallic nanoparticles were then separated magnetically (Fig. 1) and excess sodium borohydride was removed by several washings with water and ethanol. After every water and ethanol washing, a pH paper was used to make sure that the solution (containing the catalyst) was neutral in nature. The subsequent washings were stopped only when the solution was found to be pH neutral. The catalyst was then dried at 50 °C overnight using a vacuum oven.

#### Copper-palladium on carbon catalyst synthesis

Copper-palladium bimetallic nanocatalysts were synthesized using the same procedure as stated in the previous section except that the iron precursor (FeCl<sub>3</sub>), used previously, is replaced by a copper precursor

(CuCl<sub>2</sub>) keeping the mole ratio of Pd:Cu constant as before (Pd:Cu ratio 1:20). During synthesis, to make Cu particles on 100 mg carbon, 212 mg CuCl<sub>2</sub> (anhydrous) was dispersed in 30 mL water and sonicated for 10 min. The remaining procedure is the same as described in the section above.

#### Copper-iron on carbon catalyst synthesis

This catalyst was synthesized with a view to see whether noble metals could be replaced completely by transition metals to carry out the reduction of the substrate. The molar ratio of Cu:Fe was maintained at 1:1. In this case, initially 200 mg activated carbon was sonicated to remove all of the impurities present in it. Excess NaBH<sub>4</sub> (more than stoichiometric requirement) was added to the solution to ensure complete reduction of both the precursors. Then, solution of 212 mg CuCl<sub>2</sub> (anhydrous) in 30 mL water was added drop-wise to the carbon solution. After ensuring complete reduction of copper precursor to Cu(0), FeCl<sub>3</sub> solution (289.3 mg FeCl<sub>3</sub> in 30 mL water) was added to this mixture to form Cu-Fe bimetallic nanocatalysts. The remaining procedure is the same as described in the section above.

#### Catalyst characterization

The synthesized catalysts were characterized using various techniques [32–34]. Among all catalysts studied in this work, Fe-Pd bimetallic catalyst was found to be the best (as seen in Fig. 8) and was thus, characterized in further detail.

#### Scanning electron microscopy (SEM)

Surface characteristics of the catalyst were studied using SEM (JEOL, Japan, Camera SU 30 microscope). Initially, the samples to be tested were dried and then loaded on specimen studs followed by sputter coating with a thin gold film to avoid charring. Topographical images were assembled from back scattered primary or low-energy secondary electrons.

#### Transmission electron microscopy (TEM)

TEM images were taken on the JEOL JEM 2100, Japan. The images were taken at 200 kV with copper grids of 3 μm thickness. The grids were impregnated with the solid catalyst dispersed in ethanol, and then allowed to dry using UV lamp. The grid was loaded on the loading arm and the electron gun was started.

#### X-ray diffraction technique (XRD)

The X-ray scattering measurements were studied using a Bruker AXS, D8 Discover instrument with Cu-K (1.54 Å). The scattered intensities were collected from 5 to 80° (2θ) with a counting time of 0.5 s at each step.

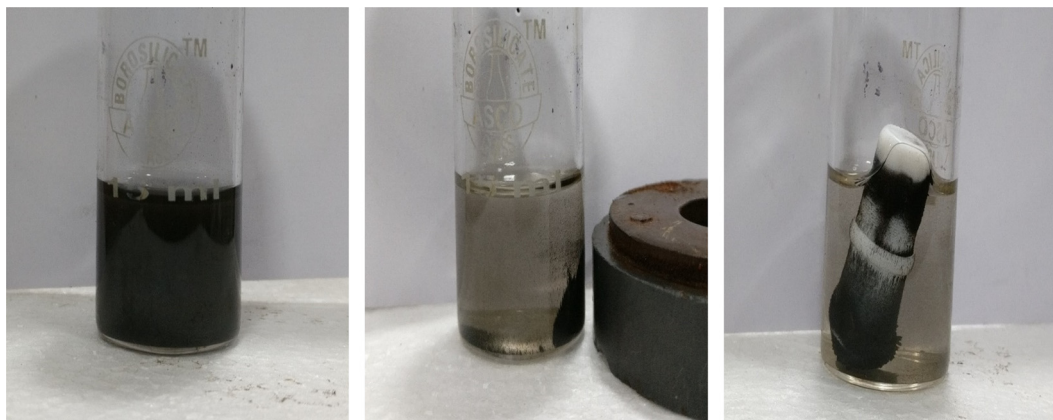


Fig. 1. Magnetically separable Fe-Pd/C bimetallic structured nanoparticles.

### Temperature programmed reduction (TPR)

Temperature programmed reduction (TPR) was performed by using a Micromeritics AutoChem 2920 (USA) instrument. 30–100 mg of sample was initially treated under helium to the temperature of 500 °C to get rid of any impurities present. The sample was flushed with helium. Temperature was then reduced to 50 °C. The sample was then given dose of hydrogen using 10% v/v H<sub>2</sub>-Ar at 500 °C and maintained there for 30 min. The temperature was brought down to 50 °C. The sample was flushed with He to remove physisorbed hydrogen and then subsequently the furnace temperature was increased from 50 to 900 °C at a heating rate of 10 °C/min under He flow. The amount of H<sub>2</sub> consumed by the sample was measured by TCD and quantified by calibration.

### Surface area and porosity analysis

The analysis of surface area and pore size distribution was carried out by using Micromeritics ASAP 2010 instrument by N<sub>2</sub> adsorption at –197 °C, after subjecting the sample to high vacuum at 450 °C for 4 h.

### X-ray photoelectron spectroscopy (XPS)

The chemical composition and oxidation state of Fe and Pd in the synthesized catalyst were studied using an XPS analysis. The analysis on the samples was performed at the CSIR-National Chemical Laboratory, Pune, India.

### Hydrogenation experiments

The hydrogenation reaction was carried out in a 100 mL Haste Alloy C autoclave (Amar Equipments Pvt Ltd, Mumbai). The autoclave was fed with appropriate quantities of HMF, internal standard (I.S.), solvent and the catalyst. The reactor was initially flushed with nitrogen to ensure that no air or oxygen was trapped in the autoclave. After achieving the desired temperature, the hydrogen pressure in the reactor was set and agitation was started. In a typical experiment, 2 mmol (0.26 g) HMF, 20 mL reaction solvent, 0.3 mL internal standard (n-decane) and 200 mg catalyst were charged into the autoclave. Samples were drawn periodically for analysis. The typical Pd metal to substrate mole ratio was 1:20 at optimized condition.

Samples were withdrawn from the reactor through a sampling port present on it by stopping the agitation momentarily. Typically, 0.5 mL

of sample would be collected free of catalyst. This sample was then subjected to centrifugation to prevent any catalyst particles from interfering with further analysis.

### Analysis

The sample was analyzed using GC (Chemito model, 1000, FID Detector) using a BP-1 capillary column. The product obtained, DMF, was confirmed using GC–MS (Perkin Elmer Clarus 500).

## Results and discussions

### Catalyst characterisation

#### Scanning electron microscopy (SEM)

Fig. 2 depicts the SEM images of Fe-Pd catalyst. The images were obtained at 1000x and 4000x magnification to indicate that the particles are nano-sized, falling in the range of 10–50 nm. It also shows that there are no agglomerates present at the surface. Fig. 2 c contains the selected area elemental analysis grayscale mapping of Fe, C and Pd. It shows the coexistence of C, Fe and Pd in the prepared material with low concentration of Pd compared to Fe on C.

#### Transmission electron microscopy (TEM)

Fig. 3 shows the transmission electron microscopy images of Fe-Pd/C catalyst at 50 nm and 10 nm resolution. It indicates the formation of nanoparticle structures. The formation of bimetallic structures of Fe-Pd atoms is also seen. The images are in concurrence with some of the previous reports [28].

#### X-ray diffraction (XRD)

The diffraction pattern for the Fe-Pd catalyst was obtained. The recycled catalyst was also characterized using XRD (Fig. 4). There is hardly any difference in the patterns of both the catalysts proving that the crystallinity fidelity are maintained.

The XRD pattern of both fresh and reused Fe-Pd/C bimetallic nanocatalyst show diffraction lines with low intensities as the particle size was small (Fig. 4). However, a distinct diffraction line is seen at around 40.01° due to the face centred cubic (FCC) structured Pd corresponding to its (111) reflections. Small lines are observed around 46° and 68°,

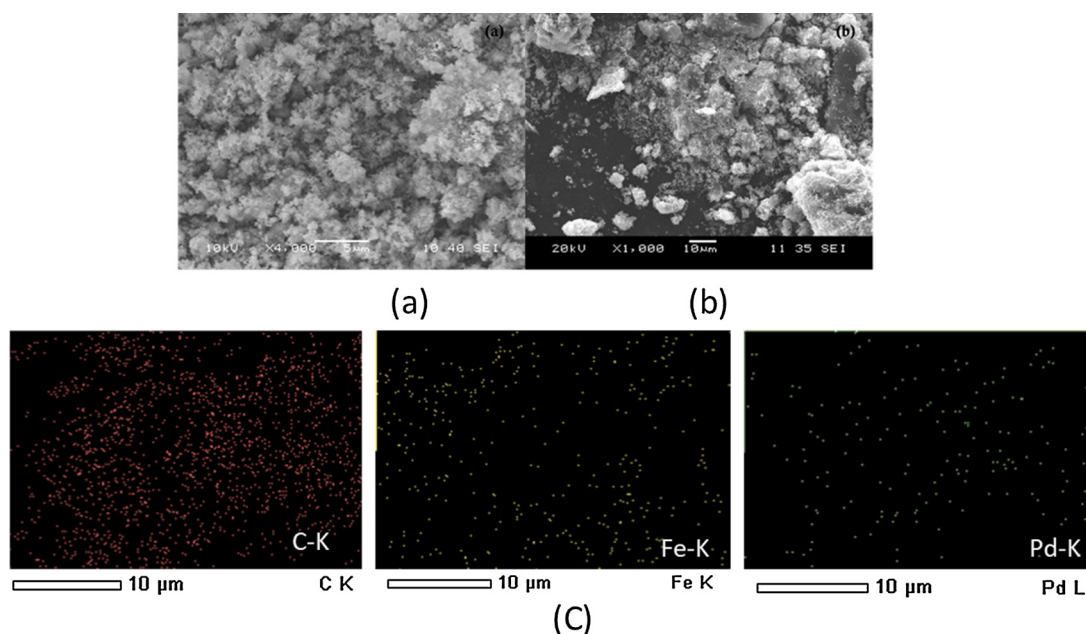


Fig. 2. SEM topography images of Fe-Pd/C catalyst. (a) at 4000x magnification and (b) at 1000x magnification (c) Elemental mapping of Fe, Pd and C on the catalyst surface.

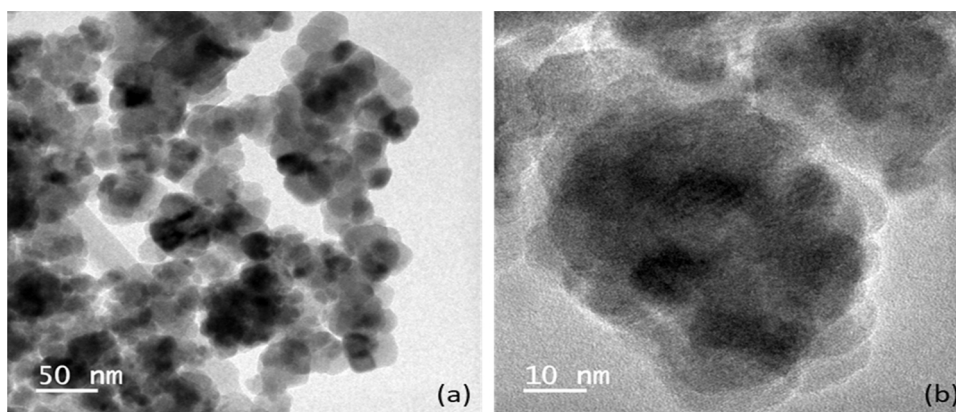


Fig. 3. TEM image of the Fe-Pd/C bimetallic structured nanocatalysts.

accounting for the Pd (200) and (220) planes [28]. The diffraction lines at around  $30.31^\circ$ ,  $35.71^\circ$ ,  $57.31^\circ$  and  $63.01^\circ$  are also observed for  $\gamma$ - $\text{Fe}_2\text{O}_3$  and/or  $\text{Fe}_3\text{O}_4$  phases ( $\text{Fe}_x\text{O}_y$ ) and these diffraction lines correspond to the reflections of planes (220), (300), (511) and (440) respectively [35]. Peak at  $43^\circ$  corresponds to presence of reduced Fe in the prepared catalyst [28,36]. This also indicates that not all Fe particles have been sacrificed to reduce Pd from  $\text{Pd}^{2+}$ . Peaks corresponding to iron and iron oxide confirm the presence of magnetic components in prepared sample. The crystallite size of Fe-Pd/C sample is 13.54 nm and of the recycled catalyst is 15.9 nm as obtained by applying the Scherrer's equation [37]. It is difficult to distinguish between the  $\gamma$ - $\text{Fe}_2\text{O}_3$  and  $\text{Fe}_3\text{O}_4$  phases using the XRD technique alone as these two phases share the same inverse spinel structure and show similar d spacing. However, finding the exact composition of these phases is not important as both these phases exhibit magnetic properties.

#### Temperature programmed reduction (TPR)

$\text{H}_2$ -TPR of bimetallic sample was performed to see the reduction behaviour and interaction between two metal species of the catalyst. For the Fe-Pd/C catalyst in consideration, Fig. 5 gives TCD signal for the catalyst versus temperature. TPR profile showed a sharp negative peak at  $80^\circ\text{C}$  corresponding to the decomposition of palladium hydrate phase i.e.  $\beta$ - $\text{PdH}_x$ , which confirms the presence of reduce Pd nanoparticle in the sample. The decomposition temperature of palladium hydrate phase ranges between  $65$ – $85^\circ\text{C}$  [38–40]. It also exhibits additional three peaks at  $360$ ,  $578$  and  $640^\circ\text{C}$ . The reduction peaks at  $360^\circ\text{C}$  corresponds to change of phase of  $\text{Fe}_2\text{O}_3$  to metallic  $\text{Fe}_3\text{O}_4$  while peaks at  $578^\circ\text{C}$  correspond to reduction of  $\text{Fe}_3\text{O}_4$  to  $\text{FeO}$ . The observed peak at  $640^\circ\text{C}$  represent the reduction of  $\text{FeO}$  to metal Fe particles. As reported earlier by Espro et al. [39], the corresponding reduction temperature for iron oxides supported on carbon is  $335^\circ\text{C}$  ( $\text{Fe}_2\text{O}_3$  to metallic  $\text{Fe}_3\text{O}_4$ ),  $495^\circ\text{C}$  ( $\text{Fe}_3\text{O}_4$  to  $\text{FeO}$ ) and  $561^\circ\text{C}$  ( $\text{FeO}$  to metal Fe) [38]. The shift in reduction temperature of different phases of Fe in

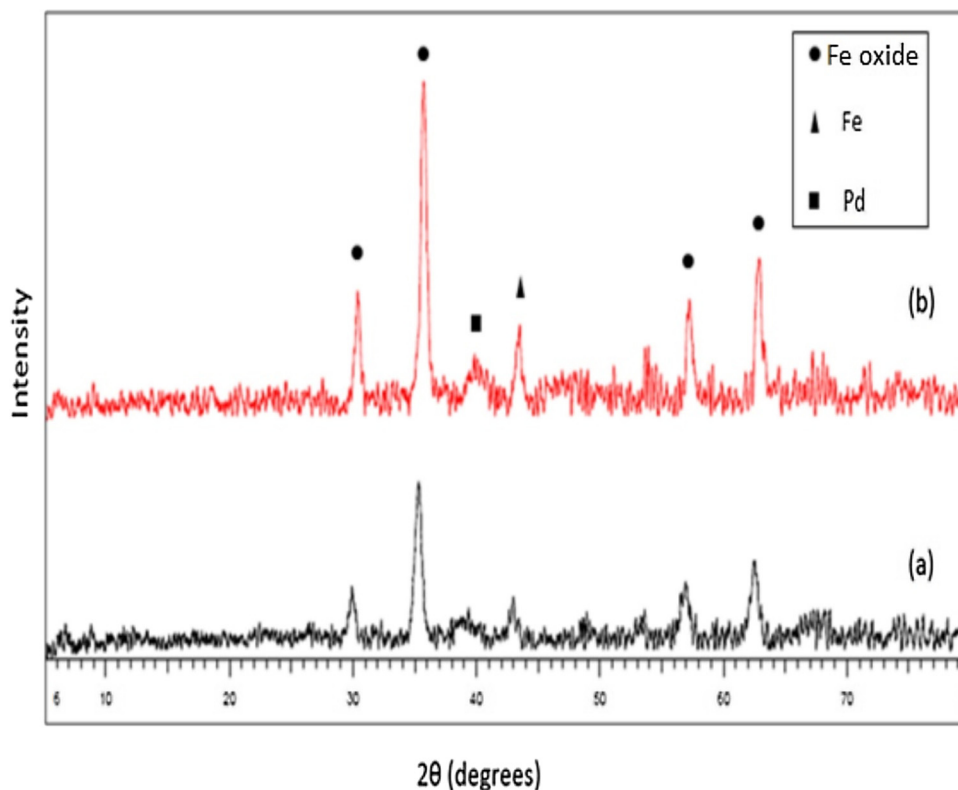


Fig. 4. XRD diffraction patterns of (a) fresh catalyst and (b) recycled catalyst.

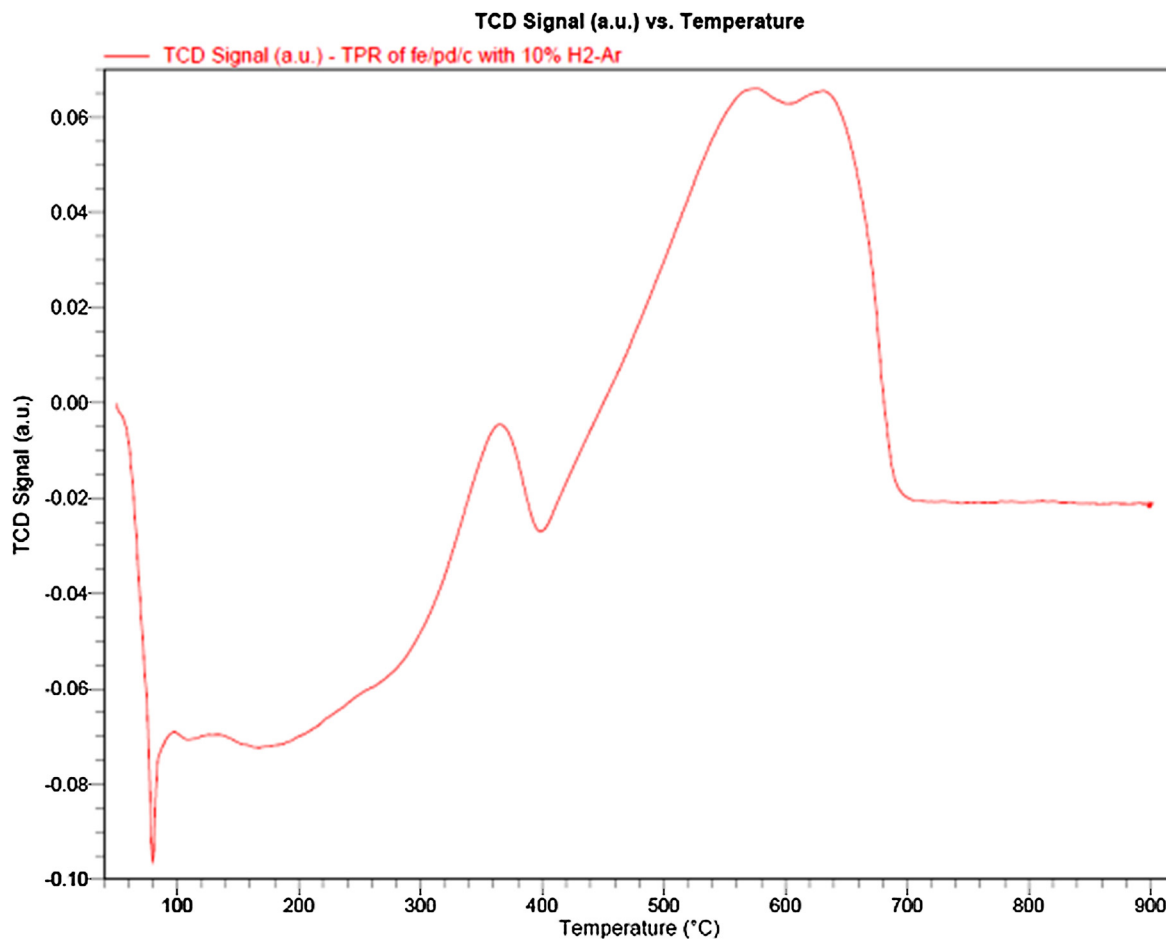


Fig. 5. H<sub>2</sub>-TPR profiles of Fe-Pd/C.

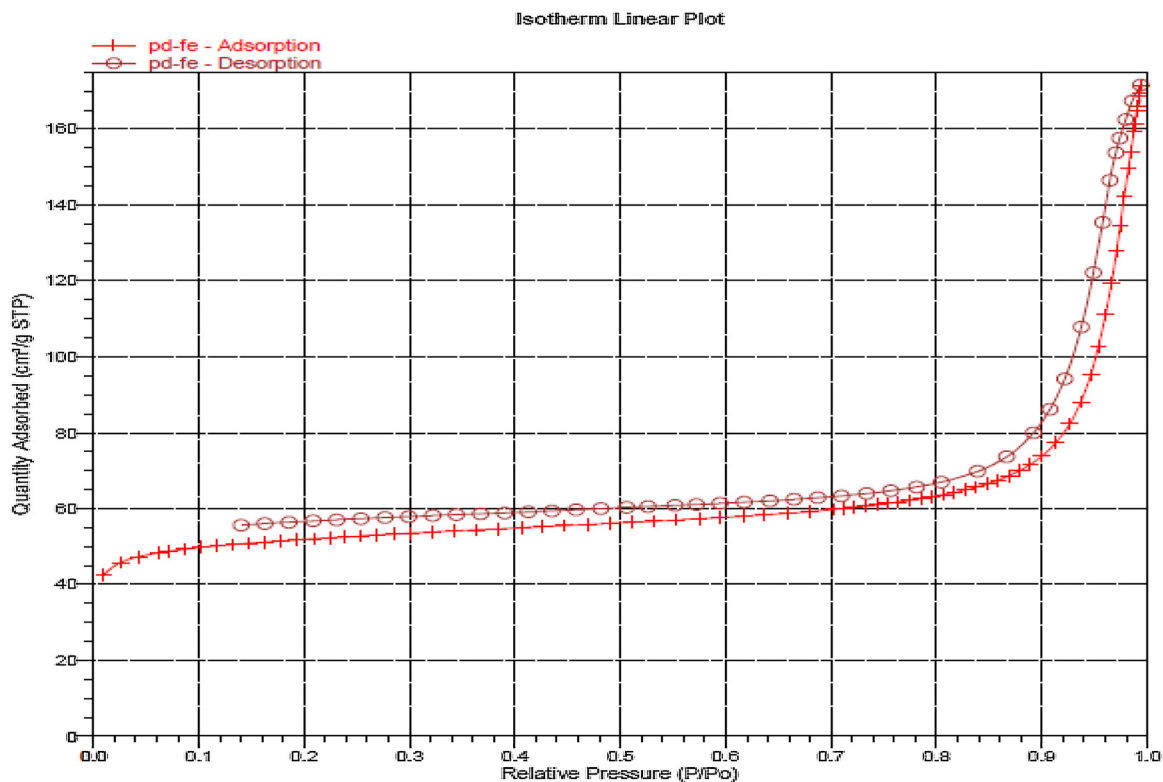


Fig. 6. Adsorption-desorption isotherm of the fresh Fe-Pd/C catalyst.

present catalyst is due to high content of Fe in the catalyst as reported earlier [39]. Usually, the presence of a noble metal (here Pd) in the bimetallic catalyst with Fe results in a decrease in the reduction temperature of Fe atoms. This is due to the interaction of two metals which can be correlated to the formation of alloys with the two metals [39,40]. Using the current synthesis method, no shifts in the reduction temperature have been observed for Fe, indicating that the alloy formation does not take place.

#### Surface area and porosity analysis

The adsorption desorption isotherms for the Fe-Pd/C catalyst with Pd:Fe 1:20 showed characteristic of microporous solids (Fig. 6).

Characteristic nitrogen BET surface area, pore size and pore volume for the fresh catalyst and the catalyst after 1<sup>st</sup> and 2<sup>nd</sup> use are given in Table 1. There is marginal change in the pore width, pore volume and the surface area of the catalyst, before and after its use, thereby proving the fidelity of the catalyst.

#### X-ray photoelectron spectroscopy (XPS)

The full elemental survey using an XPS shows the presence of oxygen, carbon, palladium and iron and no other impurities (Fig. 7a). Binding energies for the peaks at 338.1 eV and 343.1 eV can be assigned to the Pd3d electrons corresponding to the presence of Pd<sup>0</sup> state [28,41] (Fig. 7b). This confirms the presence of metallic state of Pd on the iron surface and absence of palladium oxide in the sample. Further, the peaks at different binding energies for Fe species at 706.8eV, 710.8 eV and 723.2 eV correspond to Fe<sup>0</sup> (Fe2p<sub>3/2</sub>), oxidized Fe2p<sub>3/2</sub> and Fe2p<sub>1/2</sub> electron (Fig. 7c). The shoulder at 719 eV is due to the overlapping of shakeup satellite for oxidized Fe2p<sub>3/2</sub> and Fe<sup>0</sup> (2p<sub>3/2</sub>) [42]. The peaks at 710.8 eV and 723.2eV confirm the presence of double and tri valent iron atoms in the prepared bimetallic catalyst [28,41]. The results confirm the presence of bimetallic nature of the catalyst with reduced Pd on iron oxide [28] without formation of a metal alloy.

**Table 1**

BET surface area and porosity analysis of fresh and reused catalysts.

Catalyst	BET Surface area (m <sup>2</sup> /g)	Single point adsorption pore volume (cm <sup>3</sup> /g)	Adsorption average pore width, nm
Fe-Pd	167.97	0.25	5.94
Fe-Pd 1st use	148.51	0.215	5.8
Fe-Pd 2nd use	171.20	0.224	5.2

#### Effect of different parameters on conversion and selectivity

The conversions of HMF in all cases was found to very high. Thus, to maximise the yields of DMF, it was necessary to improve the selectivity of DMF. A systematic study was undertaken to optimize the reaction parameters. The standard experiments were replicated three times and the experimental data was found to lie within a standard percentage error of 3%.

#### Catalyst screening

The hydrogenation of HMF was carried out using four different catalysts. Three of them were synthesized in the lab and other was commercially available (Fig. 8). Palladium proves to be a very efficient catalyst yielding good conversions in most of the reactions where it is employed due to its high hydrogen adsorbing capacity [43,44]

Iron is considered as a cheaper source for replacement of palladium and has been employed for application in various reduction reactions [45]. Copper metal shows good selectivity and reactivity even at lower temperatures [44]. Our main aim of preparing bimetallic combinations was to improve the desired product yield. It was observed that the commercial catalyst 5% Pd/C and the bimetallic catalyst Cu-Pd/C carried out ring hydrogenation of DMF, thereby reducing its yield. The yield observed was much higher in the case of Fe-Pd/C as compared to Cu-Fe/C. Lower activity of the latter may be due to absence of noble metal in the catalyst. Thus, Fe-Pd/C catalyst was used in further studies.

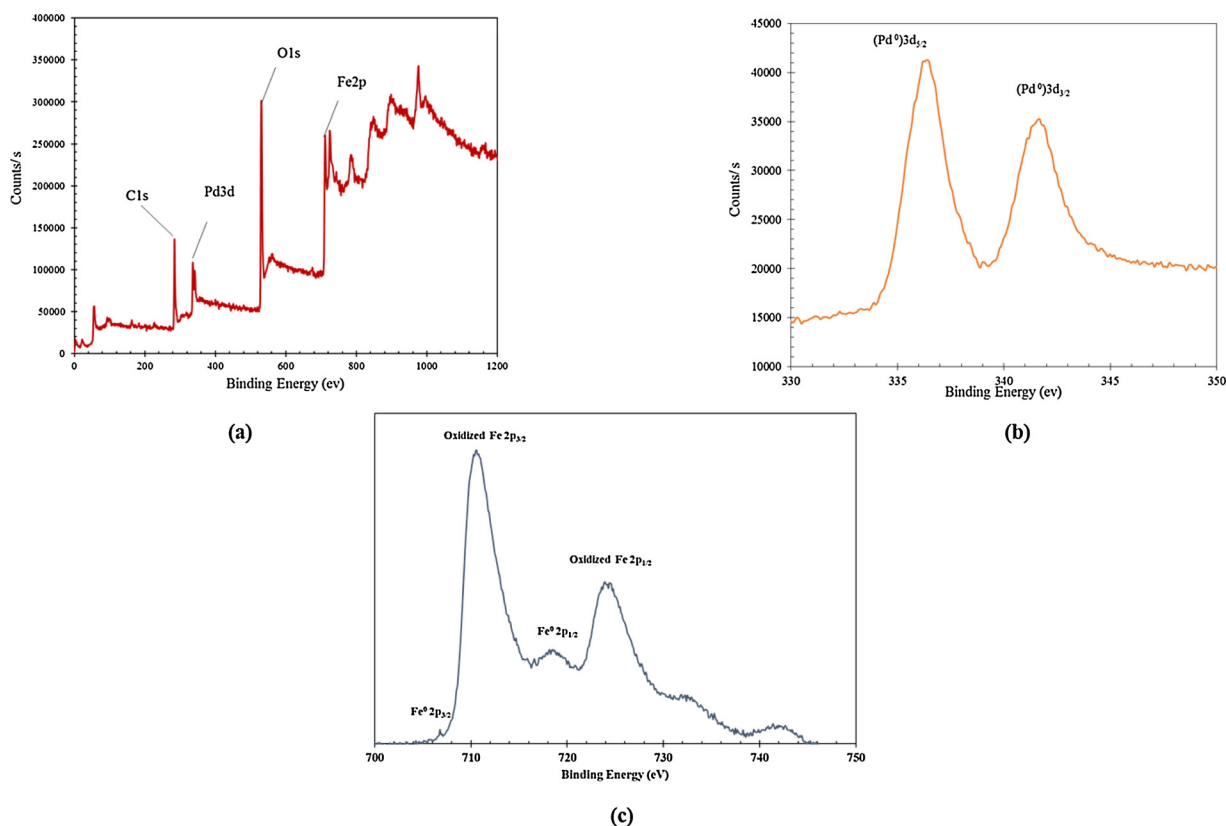
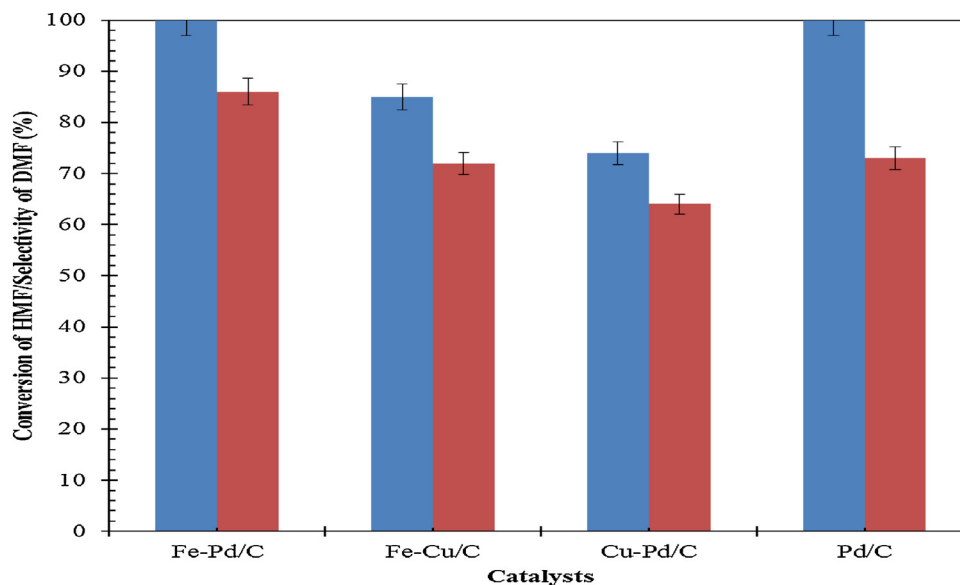


Fig. 7. XPS spectra of Fe-Pd NPs (a) full scan survey, (b) Pd 3d-electrons of palladium-containing nanoparticles, (c) Fe 2p-electrons.



**Fig. 8.** Effect of different catalysts on conversion of HMF and selectivity of DMF.

Reaction Conditions: HMF 2 mmol, THF 20 mL, IS 0.3 mL, catalyst 10 g/L, temperature 150 °C, pressure 20 bar, speed of agitation 1000 rpm.

Tetrahydrofuran was a better solvent. When n-butanol and 1, 4-dioxane were used as solvent, the analysis was very difficult. The product could not be identified due to close boiling point difference between DMF and these solvents.

#### Effect of agitation speed

The agitation speed was varied from 600 to 1200 rpm to study the effect of external mass transfer resistance (Fig. 9). Complete conversion of HMF was possible and the DMF selectivity increased, only slightly, with time when the agitation speed was increased from 600 to 1200 rpm (from 79% to 87%). Speeds higher than 1000 rpm show

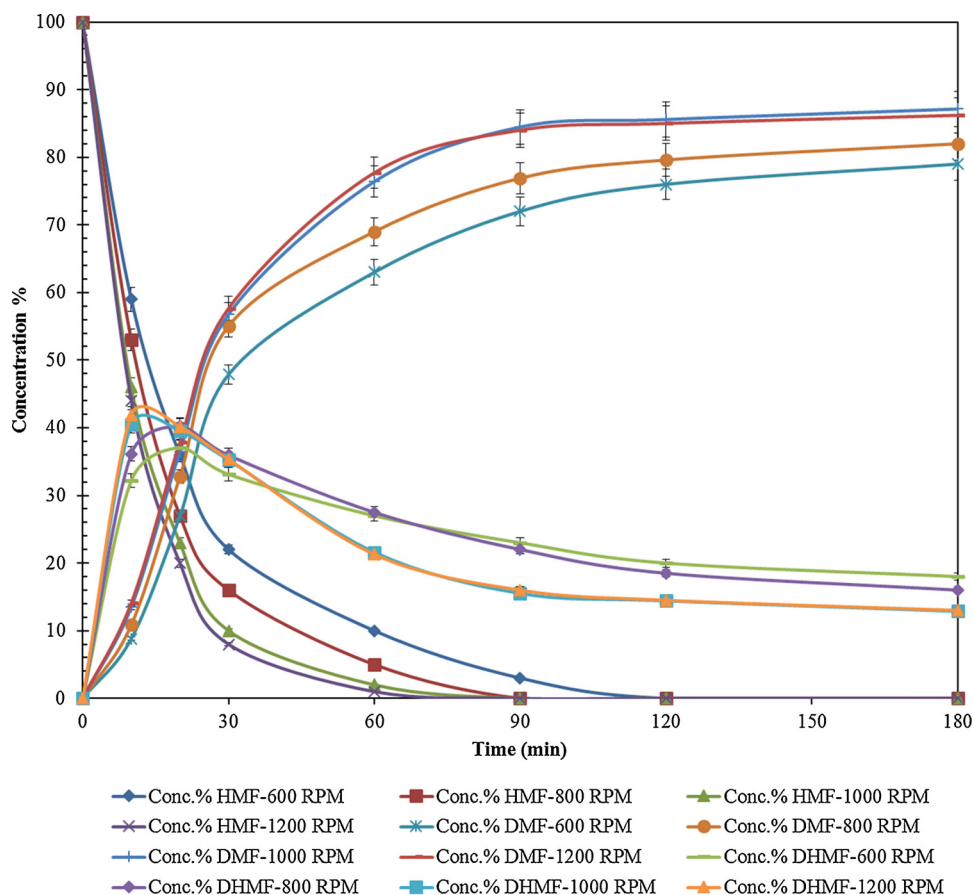


**Fig. 9.** Effect of Speed of Agitation on conversion of HMF and selectivity of DMF.

Reaction Conditions: HMF 2 mmol, THF 20 mL, IS 0.3 mL, catalyst 10 g/L, temperature 150 °C, pressure 20 bar.

minimum changes in product yield. Thus 1000 rpm was considered as the optimum speed to overcome the external mass transfer resistance. A theoretical analysis proved that there was no external mass transfer resistance as discussed in some of our earlier work [46]

#### Effect of catalyst loading

The role of catalyst loading for the selected catalyst was studied by varying the loading from 2.5 to 20 g/L (Fig. 10). As the loading of the catalyst in the reaction mixture was increased, the number of active sites increased, which led to increased initial rates of reaction. The selectivity of DMF increased from 83% at 2.5 g/L to 87.5% at 20 g/L. However, at very high catalyst loadings (higher than 10 g/L), there was no significant change in DMF yield even though the number of available sites increased. Further, the increase in catalyst amount also results in side reaction of the DMF to by-products. Thus 10 g/L was found to be the optimum catalyst loading for obtaining high yields of desired product.

#### Effect of substrate concentration

The effect of substrate concentration on DMF yield was studied by varying it from 0.05 to 0.2 mmol/mL (Fig. 11). As concentration of the substrate increased, the rate of reaction increased. Higher yield of DMF was obtained at higher substrate concentrations (from 83% at 0.05 mol/L to 88% at 0.2 mol/L). The increase in HMF concentration increases the number of HMF available and hence the rate of conversion is also increased. However, no significant increase was observed after 0.1 mol/L substrate concentration which may be due to competitive adsorption of HMF.

#### Effect of temperature

The reaction temperature is an important parameter while carrying

out the hydrogenation of HMF to DMF. At higher temperatures and pressures, it is observed that the hydrogen molecule dissociates into atomic form. Its degree of dissociation increases, thereby allowing it to bind successfully [43]. The effect of temperature was studied by varying the temperature from 130 °C to 190 °C (Fig. 12). As the temperature increased, the rate of reaction increased leading to higher conversions. The selectivity for DMF increases from 83% at 130 °C to 88% at 150 °C. After 150 °C, however, even though the reaction rate seems to be increasing, an increase in the formation of the by-products (2,5-dimethyltetrahydrofuran) occurred along with DMF. This led to reduction of DMF yield (86% at 190 °C). Thus, 150 °C was considered as the optimum condition.

#### Effect of pressure

The pressure effects were studied by varying total hydrogen pressure from 10 to 25 atm (Fig. 13). Pressure had an impact on the yield of DMF. With increase in the hydrogen pressure, the concentration of hydrogen inside the liquid phase increases which leads to higher rate of reaction. As seen, the DMF selectivity was changed significantly with increase in the hydrogen pressure from 80% at 10 atm to 88% at 20 atm. In this paper, we have performed experiments at 25 atm (highest pressure) but it was found to favour by-product formation through ring hydrogenation mechanisms leading to products such as 2, 5-dihydroxy-tetrahydrofuran (DHTHF) and 2, 5-dimethyltetrahydrofuran (DMTHF). Thus 20 atm was found to be the optimum pressure for this reaction.

#### Catalyst reusability

The catalyst reusability studies were done over three runs, including the fresh catalyst (Fig. 14). Since the catalyst was magnetically separable, it could settle in presence of the magnetic field. The catalyst was

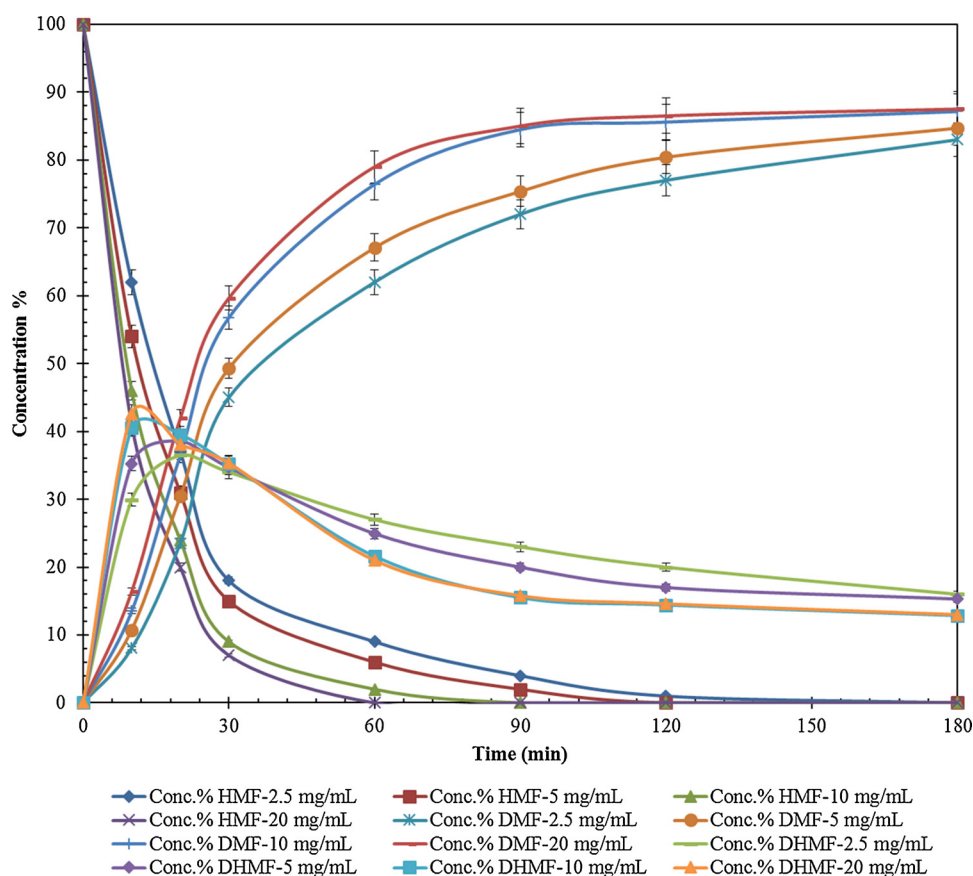
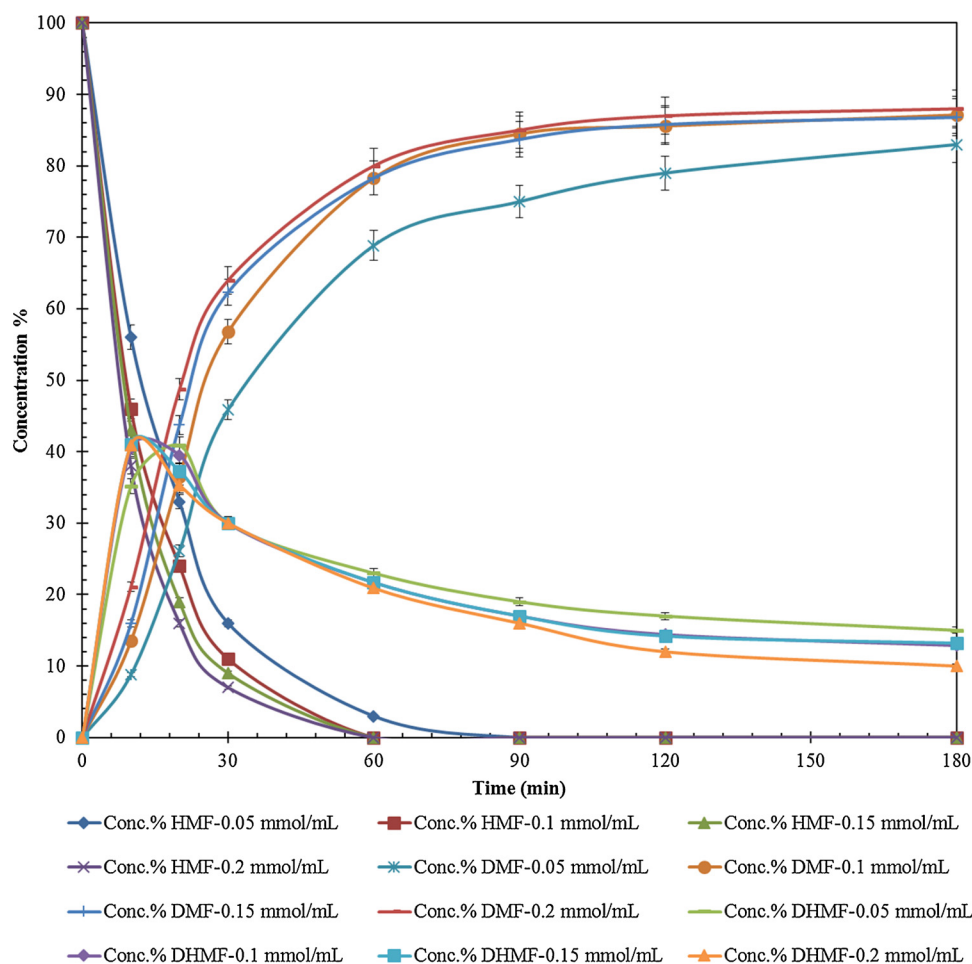


Fig. 10. Effect of Catalyst Loading on conversion of HMF and selectivity of DMF.

Reaction Conditions: HMF 2 mmol, THF 20 mL, IS 0.3 mL, temperature 150 °C, pressure 20 bar, speed of agitation 1000 rpm.



**Fig. 11.** Effect of substrate concentration on conversion of HMF and selectivity of DMF. Reaction Conditions: THF 20 mL, IS 0.3 mL, catalyst 10 g/L, temperature 150°C, pressure 20 bar, speed of agitation 1000 rpm.

separated by decanting the reaction mixture. The catalyst was then refluxed with THF to remove any adsorbed impurities and vacuum dried overnight. There is a slight loss in catalyst amount during handling. The recovered catalyst was then directly used as described in experimental section. It was observed that there was no loss in the magnetic properties of this catalyst even after consecutive uses. The slight decrease in the DMF yield is due to the decrease in the amount of catalyst fed in next cycle. Further, to test the leaching of catalyst, hot filtration test was done at same condition and the catalyst was removed after 30 min. The reaction was further carried out for 2 h at given condition. There was very slight increase in yield of DMF from 56.8% to 58.2% which can be considered as an experimental error. Thus, there is no leaching of active sites and catalyst was reusable and robust. Reused catalyst was also characterized by XRD which shows identical peaks as in the case of fresh catalyst. This confirms that there is no change in the catalyst structure and prepared catalyst is reusable and stable.

#### Kinetic modeling

##### Reaction mechanism

Hydrogenation of HMF involves series of steps. The reactant and hydrogen get absorbed on the metallic site of the catalyst. The intermediate formed then converts into the final product i.e. DMF accompanied by water release. The reaction mechanism for the reaction system is proposed (Scheme 2).

##### Development of mathematical model

Preliminary interpretation of the rate data suggested that the

reaction follows the Langmuir-Hinshelwood-Hougen-Watson (LHHW) type model.

While considering this model, the following assumptions were made:

- 5-Hydroxymethyl furfural (HMF) and hydrogen adsorb on the adjacent metallic site.
- Hydrogen adsorbs by dissociative mechanism.

A general derivation for the hydrogenation of the substrate is attempted by using a mono-functional catalyst that contains only one type of active site 'S'. The substrate and hydrogen, both, are assumed to be adsorbed on this active site.

##### Adsorption of HMF

Chemisorption of HMF (A) on site S can be shown as:



The rate of this above chemisorption reaction is given by,

$$r_{AD} = k_a C_A C_S - k'_a C_{AS} = k_a \left( C_A C_S - \frac{C_{AS}}{K_A} \right) \quad (2)$$

##### Adsorption of hydrogen

Assuming dissociative adsorption of  $H_2$



The rate for the above reaction can be written as:

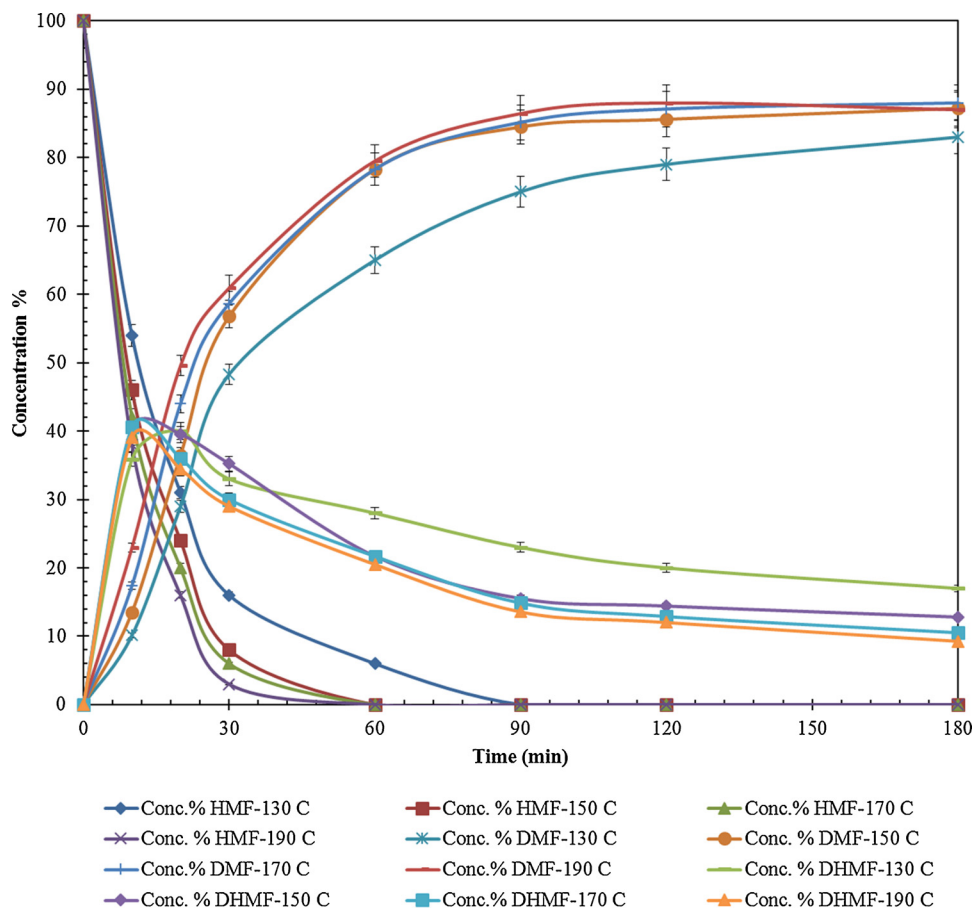


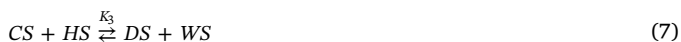
Fig. 12. Effect of Temperature on conversion of HMF and selectivity of DMF.

Reaction Conditions: HMF 2 mmol, THF 20 mL, IS 0.3 mL, catalyst 10 g/L, pressure 20 bar, speed of agitation 1000 rpm.

$$r_{HD} = k_h P_{H_2} C_S^2 - k'_h C_{HS}^2 = k_h (P_{H_2} C_S^2 - \frac{C_{HS}^2}{K_H}) = k_h (P_{H_2} C_S^2 - \frac{C_{HS}^2}{K_H}) \quad (4)$$

Surface reaction

It is a series reaction wherein the intermediate is ultimately converted into the final product. The first hydrogen atom attacks the aldehyde end of the HMF molecule as shown in the mechanism leading to the formation of the first intermediate (Scheme 2). This first intermediate is then subject to hydrogenation again thereby yielding the second intermediate which gets ultimately hydrogenated to the final product.



The rates of the above equation are given as follows:

$$-r_1 = k_1 C_{AS} C_{HS} - k'_1 C_{BS} C_S \quad (8)$$

$$-r_2 = k_2 C_{BS} C_{HS} - k'_2 C_{CS} C_{WS} \quad (9)$$

$$-r_3 = k_3 C_{CS} C_{HS} - k'_3 C_{DS} C_{WS} \quad (10)$$

We assume that this step of conversion, second intermediate to the final product, is the slower of the two and hence the rate determining step. Thus, the controlling rate Eq. (10) can be modified to,

$$-r_3 = k_3 C_{CS} C_{HS} \quad (11)$$

The other two reaction steps are thus considered to be fast and in equilibrium.

Thus Eq. (8) reduces to:

$$C_{BS} = K_1 \frac{C_{AS} C_{HS}}{C_S} \quad (12)$$

And from Eq. (9) reduces to,

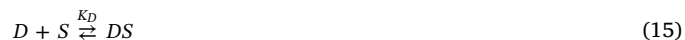
$$C_{CS} = K_1 \frac{C_{BS} C_{HS}}{C_{WS}} \quad (13)$$

The controlling rate then reduces to

$$-r_3 = k_3 K_1 K_2 \frac{C_{AS} C_{HS}^3}{C_S C_{WS}} \quad (14)$$

Desorption

For the sake of simplicity, we have assumed only one product, final product i.e. 'D'.



Desorption rate can be written as:

$$-r_D = k_d (C_{DS} - \frac{C_D C_S}{K_D}) \quad (16)$$

As the surface reaction is the rate-controlling step, the other steps (adsorption and desorption) can be considered to be fast and in equilibrium.

Thus Eq. (2) becomes,

$$k_a C_A C_S = k'_a C_{AS} \quad (17)$$

$$C_{AS} = \frac{k_a C_A C_S}{k'_a} \quad (18)$$

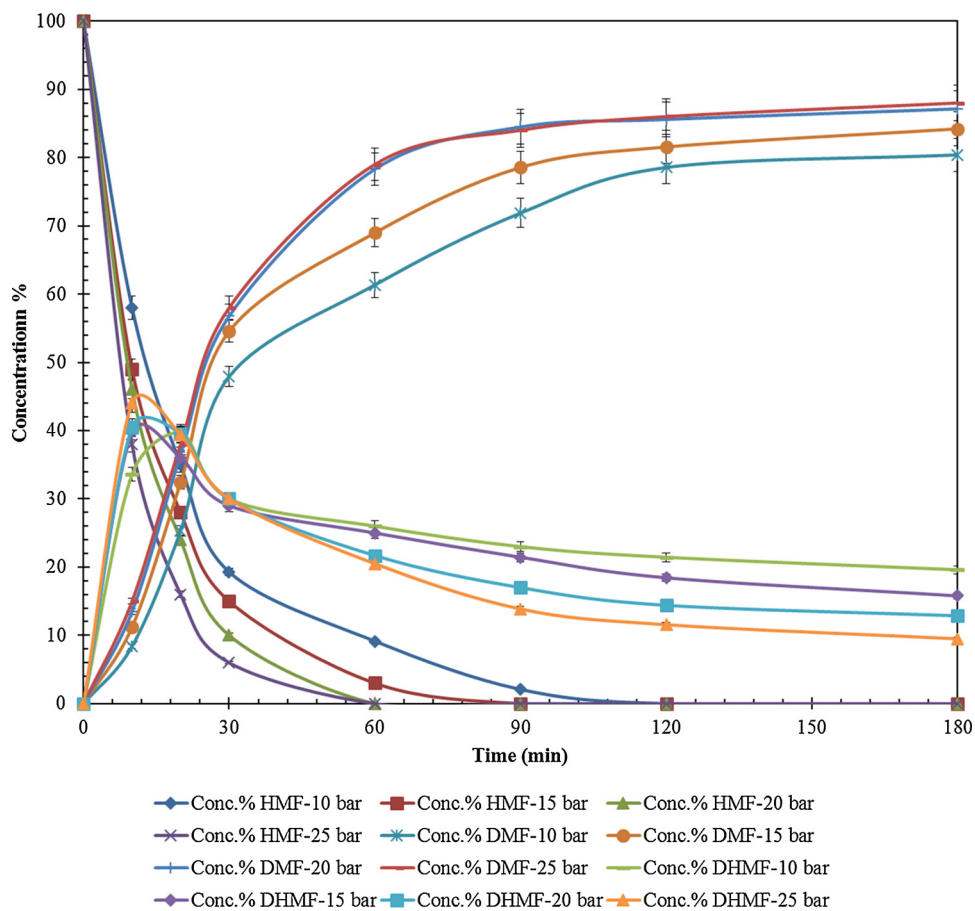


Fig. 13. Effect of Pressure on conversion of HMF and selectivity of DMF. Reaction Conditions: HMF 2 mmol, THF 20 mL, IS 0.3 mL, catalyst 10 g/L, temperature 150 °C, speed of agitation 1000 rpm.

$$C_{AS} = K_A C_A C_S \tag{19}$$

$$C_{HS}^2 = K_H P_{H_2} C_S^2 \tag{20}$$

Also, Eq. (4) becomes,

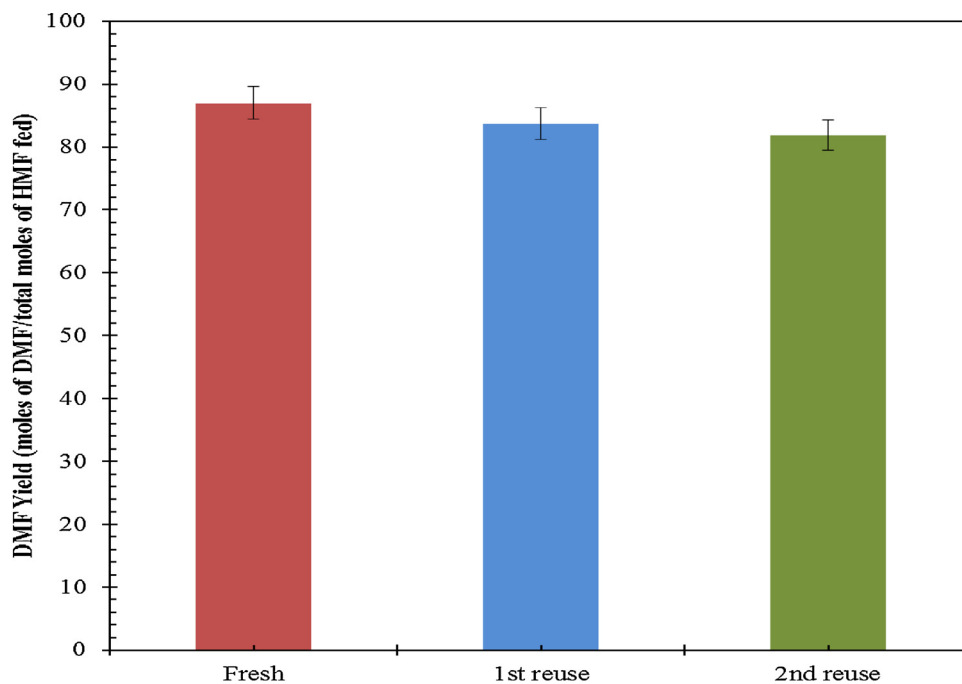
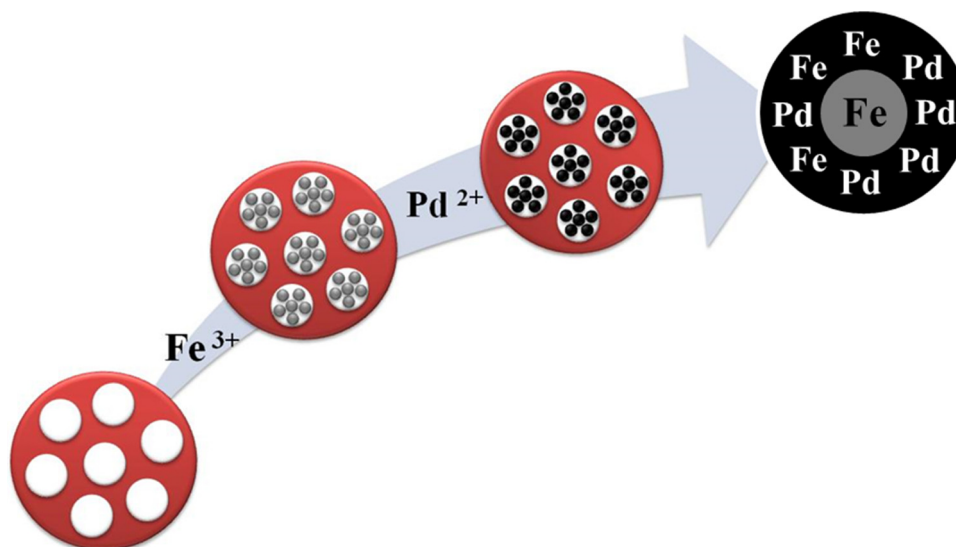


Fig. 14. Effect of Catalyst Reusability on yield of DMF. Reaction Conditions: HMF 2 mmol, THF 20 mL, IS 0.3 mL, catalyst 10 g/L, temperature 150 °C, pressure 20 bar, speed of agitation 1000 rpm.



**Scheme 2.** Possible mechanism for transformation of HMF to DMF.

**Table 2**

Value of kinetic rate constants at different temperatures.

Temp (°C)	Rate constant, $k_p'$ (L <sup>2</sup> /mol/g. cat/min)	Adsorption equilibrium constant, $K_A$ (L/mol)	Adsorption equilibrium constant, $K_H$ (L/mol)
80	1.49E-02	5.9E-03	6.017
100	6E-02	5.3E-03	5.76
120	1E-01	4.7E-03	5.17
140	1.76E-01	4.3E-03	4.21

$$C_{HS} = \sqrt{K_H P_{H_2}} C_S \quad (21)$$

Desorption step is also considered to be in equilibrium. Thus Eq. (16) becomes

$$C_{DS} = K_D C_D C_S \quad (22)$$

Similarly, for water, we can write a similar equation:

$$C_{WS} = K_W C_W C_S \quad (23)$$

The total balance for the catalytic sites can be written as follows:

$$C_T = C_S + C_{AS} + C_{HS} + C_{DS} + C_{WS} \\ = C_S (1 + K_A C_A + \sqrt{K_H P_{H_2}} + K_D C_D + K_W C_W) \quad (24)$$

$$C_S = \frac{C_T}{(1 + K_A C_A + \sqrt{K_H P_{H_2}} + K_D C_D + K_W C_W)} \quad (25)$$

The controlling rate from Eq. (14) can now be converted to all the known concentrations.

$$-r_3 = k_3 K_1 K_2 \frac{C_{AS} C_{HS}^3}{C_S C_{WS}} \quad (26)$$

Substituting values from above equations, we get,

$$-r_3 = \frac{(k_3 K_1 K_2 K_A C_A K_H^{3/2} P_{H_2}^{3/2}) C_S^2}{K_W C_W} \quad (27)$$

Substituting the value of  $C_S$  from Eq. (25), the following is obtained:

$$-r_3 = \frac{(k_3 K_1 K_2 K_A C_A K_H^{3/2} P_{H_2}^{3/2}) C_T^2}{K_W C_W (1 + K_A C_A + \sqrt{K_H P_{H_2}} + K_D C_D + K_W C_W)^2} \quad (28)$$

Since it is assumed that the surface reaction is rate controlling, the desorption constant will be low. Thus, the above equation reduces to,

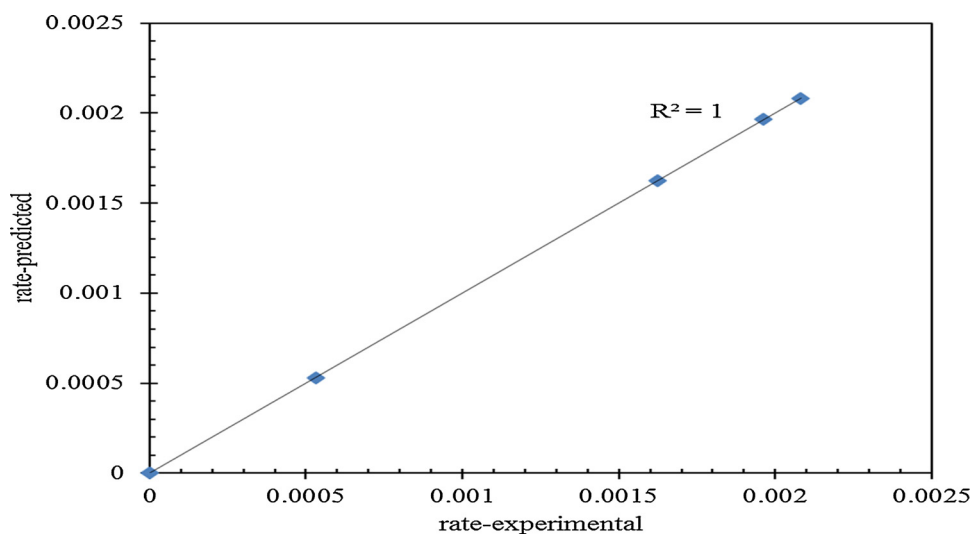


**Fig. 15.** Parity plot.

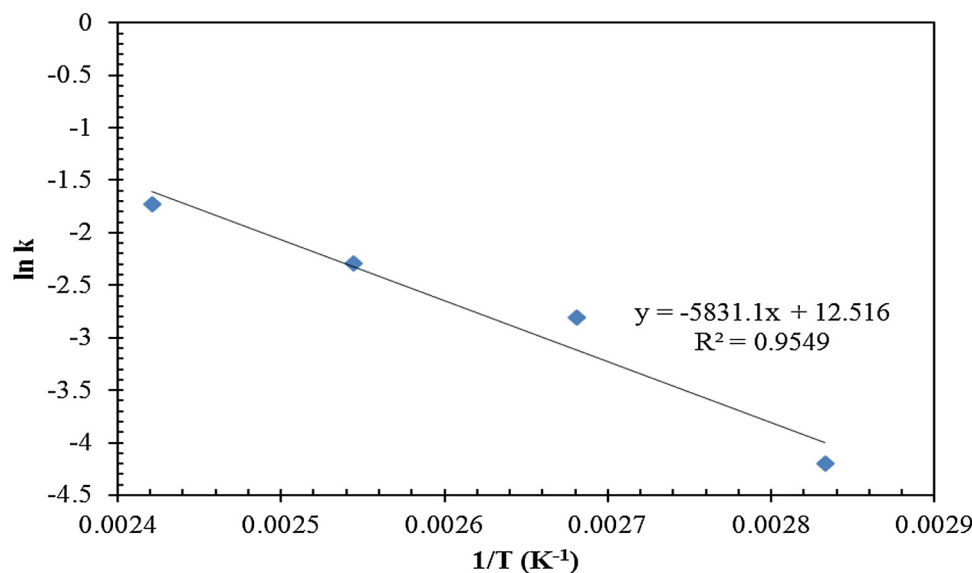


Fig. 16. Arrhenius plot.

$$-r_A = \frac{dC_D}{dt} = \frac{(kK_A K_H^{3/2} P_{H_2}^{3/2}) C_A w}{K_W C_W (1 + K_A C_A + \sqrt{K_H P_{H_2}} + K_D C_D + K_W C_W)^2} \quad (29)$$

Where,  $k = k_3 K_1 K_2$  and  $w$  is the catalyst loading.

Eq. (29) can be solved for obtaining values of the kinetic rate constant and adsorption coefficients (Table 2). The parity plot shows that the model developed fits the experiment data well (Fig. 15).

The high values of adsorption coefficient of hydrogen are due to the presence of noble metals. Low values are obtained for adsorption coefficients of the main reactant (i.e. HMF) and water. The rate equation can thus be simplified as follows:

$$-r_A = \frac{-dC_A}{dt} = (k' K_A \sqrt{K_H P_{H_2}}) C_A w \quad (30)$$

$$-r_A = \frac{-dC_A}{dt} = k' C_A w \quad (31)$$

Where, for constant pressure,

$$k' = k' K_A \sqrt{K_H P_{H_2}} \quad (32)$$

Thus Eq. (30) simplifies to a pseudo-first order equation (31). Using the values of kinetic rate constants, the activation energy of the reaction can be evaluated. The Arrhenius plot for the reaction was made to get the apparent energy of activation as 11.6 kcal/mol (Fig. 16).

## Conclusion

A variety of bimetallic nanoparticles comprising Fe-Pd/C, Cu-Pd/C and Cu-Fe/C were synthesized. Magnetically separable Fe-Pd/C bimetallic nano-catalyst was successfully synthesized and the characterization of the fresh and used catalyst was carried out and the fidelity of the catalyst proved. Various parameters affecting the yield of DMF have been studied successfully. We have been successful in obtaining high conversions and selectivity without the use of acidic precursors, thus making the process green. The conversions of HMF obtained are very high (> 95%) with high selectivity towards DMF (> 85%). Optimum conditions needed to obtain maximum yield of DMF were established. A mechanism for the hydrogenation reaction of HMF was postulated. The reaction system follows the LHHW type model and the experimental data fit this model well. The values for the reaction rate constants and adsorption coefficients were established. The value of activation energy was evaluated using Arrhenius plot as 11.6 kcal/mol. The reaction is kinetically controlled.

## Conflict of interest statement

The authors declare no conflict of interest.

## Acknowledgements

A.D. Talpade acknowledges University Grants Commission (UGC) for the award of UGC- Junior Research Fellowship. M. S. Tiwari acknowledges University Grants Commission (UGC) for the award of BSR Senior Research Fellowship under its SAP Program in Chemical Engineering. G.D. Yadav acknowledges support from R.T. Mody Distinguished Professor Endowment, Tata Chemicals Darbari Seth Distinguished Professor of Leadership and Innovation, and J.C. Bose National Fellowship of Department of Science and Technology, Govt. of India.

## References

- [1] Y.J. Wang, B. Bin Ying, M. Chen, W. Shen, Z.Q. Liu, An NADPH-dependent *Lactobacillus composti* short-chain dehydrogenase/reductase: characterization and application to (R) - 1-phenylethanol synthesis, *World J. Microbiol. Biotechnol.* (2017), <https://doi.org/10.1007/s11274-017-2311-9>.
- [2] Y. Zhang, Y. Chen, J. Pan, M. Liu, P. Jin, Y. Yan, Synthesis and evaluation of acid-base bi-functionalized SBA-15 catalyst for biomass energy conversion, *Chem. Eng. J.* 313 (2017) 1593–1606, <https://doi.org/10.1016/j.cej.2016.11.033>.
- [3] R. García-Morales, O. Elizalde-Solis, A. Zúñiga-Moreno, C. Bouchot, F.I. Gómez-Ramos, M.G. Arenas-Quevedo, Volumetric properties of 2,5-dimethylfuran in mixtures with octane or dodecane from 293 K to 393 K and pressures up to 70 MPa, *Fuel* 209 (2017) 299–308, <https://doi.org/10.1016/j.fuel.2017.07.112>.
- [4] E.-S. Kang, D.W. Chae, B. Kim, Y.G. Kim, Efficient preparation of DHMF and HMFA from biomass-derived HMF via a Cannizzaro reaction in ionic liquids, *J. Ind. Eng. Chem.* 18 (2012) 174–177, <https://doi.org/10.1016/j.jiec.2011.11.020>.
- [5] Z. Yang, W. Qi, R. Huang, J. Fang, R. Su, Z. He, Functionalized silica nanoparticles for conversion of fructose to 5-hydroxymethylfurfural, *Chem. Eng. J.* 296 (2016) 209–216, <https://doi.org/10.1016/j.cej.2016.03.084>.
- [6] W. Zhao, W. Wu, H. Li, C. Fang, T. Yang, Z. Wang, C. He, S. Yang, Quantitative synthesis of 2,5-bis(hydroxymethyl)furan from biomass-derived 5-hydroxymethylfurfural and sugars over reusable solid catalysts at low temperatures, *Fuel* 217 (2018) 365–369, <https://doi.org/10.1016/j.fuel.2017.12.069>.
- [7] A.B. Gawade, M.S. Tiwari, G.D. Yadav, Biobased green process: selective hydrogenation of 5-hydroxymethylfurfural to 2,5-dimethyl furan under mild conditions using Pd-Cs 2.5 H 0.5 PW 12 O 40 /K-10 Clay, *ACS Sustain. Chem. Eng.* 4 (2016) 4113–4123, <https://doi.org/10.1021/acssuschemeng.6b00426>.
- [8] J. Wang, J. Ren, X. Liu, G. Lu, Y. Wang, High yield production and purification of 5-hydroxymethylfurfural, *AIChE J.* 59 (2013) 2558–2566, <https://doi.org/10.1002/aic.14019>.
- [9] J. Shi, Y. Wang, X. Yu, W. Du, Z. Hou, Production of 2,5-dimethylfuran from 5-hydroxymethylfurfural over reduced graphene oxides supported Pt catalyst under mild conditions, *Fuel* 163 (2016) 74–79, <https://doi.org/10.1016/j.fuel.2015.09.047>.

- [10] Y. Roman-Leshkov, C.J. Barrett, Z.Y. Liu, J.A. Dumesic, Production of dimethylfuran for liquid fuels from biomass-derived carbohydrates, *Nature* 447 (2007) 982–986, <https://doi.org/10.1038/nature05923>.
- [11] T. Thananattananachon, T.B. Rauchfuss, Efficient production of the liquid fuel 2,5-dimethylfuran from fructose using formic acid as a reagent, *Angew. Chem. Int. Ed.* 49 (2010) 6616–6618, <https://doi.org/10.1002/anie.201002267>.
- [12] M. Chidambaram, A.T. Bell, A two-step approach for the catalytic conversion of glucose to 2,5-dimethylfuran in ionic liquids, *Green Chem.* 12 (2010) 1253, <https://doi.org/10.1039/c004343e>.
- [13] L. Maat, H. van Bekkum, G.C.A. Luijckx, N.P.M. Huck, F. van Rantwijk, Ether formation in alcoholic solution, *Heterocycles* 77 (2009) 1037, [https://doi.org/10.3987/COM-08-S\(F\)81](https://doi.org/10.3987/COM-08-S(F)81).
- [14] C.M. Mani, M. Braun, V. Molinari, M. Antonietti, N. Fechner, A high-throughput composite catalyst based on nickel carbon cubes for the hydrogenation of 5-hydroxymethylfurfural to 2,5-dimethylfuran, *ChemCatChem* 9 (2017) 3388–3394, <https://doi.org/10.1002/cctc.201700506>.
- [15] R. Goyal, B. Sarkar, A. Bag, N. Siddiqui, D. Dumbre, N. Lucas, S. Kumar, A. Bordoloi, Studies of synergy between metal – support interfaces and selective hydrogenation of HMF to DMF in water, *J. Catal.* 340 (2016) 248–260, <https://doi.org/10.1016/j.jcat.2016.05.012>.
- [16] G.-H. Wang, J. Hilgert, F.H. Richter, F. Wang, H.-J. Bongard, B. Spliethoff, C. Weidenthaler, F. Schüth, Platinum–cobalt bimetallic nanoparticles in hollow carbon nanospheres for hydrogenolysis of 5-hydroxymethylfurfural, *Nat. Mater.* 13 (2014) 293–300, <https://doi.org/10.1038/nmat3872>.
- [17] S. Nishimura, N. Ikeda, K. Ebitani, Selective hydrogenation of biomass-derived 5-hydroxymethylfurfural (HMF) to 2,5-dimethylfuran (DMF) under atmospheric hydrogen pressure over carbon supported PdAu bimetallic catalyst, *Catal. Today* 232 (2014) 89–98, <https://doi.org/10.1016/j.cattod.2013.10.012>.
- [18] B. Chen, F. Li, Z. Huang, G. Yuan, Carbon-coated Cu-Co bimetallic nanoparticles as selective and recyclable catalysts for production of biofuel 2,5-dimethylfuran, *Appl. Catal. B Environ.* 200 (2017) 192–199, <https://doi.org/10.1016/j.apcatb.2016.07.004>.
- [19] P. Yang, Q. Xia, X. Liu, Y. Wang, Catalytic transfer hydrogenation/hydrogenolysis of 5-hydroxymethylfurfural to 2,5-dimethylfuran over Ni-Co/C catalyst, *Fuel* 187 (2017) 159–166, <https://doi.org/10.1016/j.fuel.2016.09.026>.
- [20] J. Chen, X. Liu, F. Zhang, Composition regulation of bimetallic RuPd catalysts supported on porous alumina spheres for selective hydrogenation, *Chem. Eng. J.* 259 (2015) 43–52, <https://doi.org/10.1016/j.cej.2014.07.049>.
- [21] P.S. Kumbhar, M.R. Kharkar, G.D. Yadav, R.A. Rajadhyaksha, Geometric and electronic effects in silica supported bimetallic nickel–copper and nickel–iron catalysts for liquid-phase hydrogenation of acetophenone and benzonitrile, *J. Chem. Soc. Chem. Commun.* (1992) 584–586, <https://doi.org/10.1039/C39920000584>.
- [22] G.D. Yadav, M.R. Kharkar, Liquid-phase hydrogenation of saturated and unsaturated nitriles: Activities and selectivities of bimetallic nickel–copper and nickel–iron catalysts supported on silica, *Appl. Catal. A Gen.* 126 (1995) 115–123, [https://doi.org/10.1016/0926-860X\(95\)00039-9](https://doi.org/10.1016/0926-860X(95)00039-9).
- [23] G.D. Yadav, Y.S. Lawate, Hydrogenation of styrene oxide to 2-phenyl ethanol over polyurea microencapsulated mono- and bimetallic nanocatalysts: activity, selectivity, and kinetic modeling, *Ind. Eng. Chem. Res.* 52 (2013) 4027–4039, <https://doi.org/10.1021/ie302587j>.
- [24] G.D. Yadav, Y.S. Lawate, Selective hydrogenation of styrene oxide to 2-phenyl ethanol over polyurea supported Pd–Cu catalyst in supercritical carbon dioxide, *J. Supercrit. Fluids* 59 (2011) 78–86, <https://doi.org/10.1016/j.supflu.2011.08.008>.
- [25] J.W. Hong, D. Kim, Y.W. Lee, M. Kim, S.W. Kang, Atomic-distribution-dependent electrocatalytic activity of Au – Pd, *Angew. Chem.—Int. Ed.* (2011) 8876–8880, <https://doi.org/10.1002/anie.201102578>.
- [26] S.E. Habas, H. Lee, V. Radmilovic, G.A. Somorjai, P. Yang, Shaping binary metal nanocrystals through epitaxial seeded growth, *Nat. Mater.* 6 (2007) 692–697, <https://doi.org/10.1038/nmat1957>.
- [27] X. Liu, D. Wang, Y. Li, Synthesis and catalytic properties of bimetallic nanomaterials with various architectures, *Nano Today* 7 (2012) 448–466, <https://doi.org/10.1016/j.nantod.2012.08.003>.
- [28] W. Tang, J. Li, X. Jin, J. Sun, J. Huang, R. Li, Magnetically recyclable Fe@Pd/C as a highly active catalyst for Suzuki coupling reaction in aqueous solution, *Catal. Commun.* 43 (2014) 75–78, <https://doi.org/10.1016/j.catcom.2013.09.001>.
- [29] S.C. Patankar, G.D. Yadav, Cascade engineered synthesis of  $\gamma$ -valerolactone, 1,4-pentanediol, and 2-methyltetrahydrofuran from levulinic acid using Pd–Cu/ZrO<sub>2</sub> catalyst in water as solvent, *ACS Sustain. Chem. Eng.* 3 (2015) 2619–2630, <https://doi.org/10.1021/acsuschemeng.5b00763>.
- [30] S.C. Patankar, S.K. Dodiya, G.D. Yadav, Cascade engineered synthesis of ethyl benzyl acetoacetate and methyl isobutyl ketone (MIBK) on novel multifunctional catalyst, *J. Mol. Catal. A Chem.* 409 (2015) 171–182, <https://doi.org/10.1016/j.molcata.2015.08.018>.
- [31] M.S. Tiwari, A.B. Gawade, G.D. Yadav, Magnetically separable sulfated zirconia as highly active acidic catalysts for selective synthesis of ethyl levulinate from furfuryl alcohol, *Green Chem.* 19 (2017) 963–976, <https://doi.org/10.1039/C6GC02466A>.
- [32] M.S. Tiwari, G.D. Yadav, Novel aluminium exchanged dodecatungstophosphoric acid supported on K-10 clay as catalyst: benzoylation of diphenyl oxide with benzoic anhydride, *RSC Adv.* 6 (2016) 49091–49100, <https://doi.org/10.1039/C6RA05379C>.
- [33] M.S. Tiwari, G.D. Yadav, Kinetics of Friedel–Crafts benzoylation of veratrole with benzoic anhydride using Cs<sub>2</sub>5H<sub>0</sub>5PW<sub>12</sub>O<sub>40</sub>/K-10 solid acid catalyst, *Chem. Eng. J.* 266 (2015) 64–73, <https://doi.org/10.1016/j.cej.2014.12.043>.
- [34] M.S. Tiwari, T. Jain, G.D. Yadav, Novel bifunctional palladium–dodecatungstophosphoric acid supported on titania nanotubes: one-pot synthesis of n-pentyl tetrahydrofurfuryl ether from Furfuryl alcohol and n-pentanol, *Ind. Eng. Chem. Res.* (2017) 12909–12919, <https://doi.org/10.1021/acs.iecr.7b00078>.
- [35] K. Mori, Y. Kondo, H. Yamashita, Synthesis and characterization of FePd magnetic nanoparticles modified with chiral BINAP ligand as a recoverable catalyst vehicle for the asymmetric coupling reaction, *Phys. Chem. Chem. Phys.* 11 (2009) 8949, <https://doi.org/10.1039/b910069e>.
- [36] E.V. Golubina, E.S. Lokteva, T.S. Lazareva, B.G. Kostyuk, V.V. Lunin, V.I. Simagina, I.V. Stoyanova, Hydrodechlorination of tetrachloromethane in the vapor phase in the presence of Pd–Fe/sibunit catalysts, *React. Kinet. Catal. Lett.* 45 (2004) 183–188, <https://doi.org/10.1023/B:KICA.0000023789.28190.1b>.
- [37] U. Holzwarth, N. Gibson, The Scherrer equation versus the “Debye–Scherrer equation,” *Nat. Nanotechnol.* 6 (2011), <https://doi.org/10.1038/nnano.2011.145> 534–534.
- [38] J.K. Kim, J.K. Lee, K.H. Kang, J.W. Lee, I.K. Song, Catalytic decomposition of phenethyl phenyl ether to aromatics over Pd–Fe bimetallic catalysts supported on ordered mesoporous carbon, *J. Mol. Catal. A Chem.* 410 (2015) 184–192.
- [39] C. Espro, B. Gumina, E. Paone, F. Mauriello, Upgrading lignocellulosic biomasses: hydrogenolysis of platform derived molecules promoted by heterogeneous Pd–Fe catalysts, *Catalysts* 7 (2017) 78, <https://doi.org/10.3390/catal7030078>.
- [40] J.K. Kim, J.K. Lee, K.H. Kang, J.C. Song, I.K. Song, Selective cleavage of C–O bond in benzyl phenyl ether to aromatics over Pd–Fe bimetallic catalyst supported on ordered mesoporous carbon, *Appl. Catal. A Gen.* 498 (2015) 142–149, <https://doi.org/10.1016/j.apcata.2015.03.034>.
- [41] K. Mishra, N. Basavegowda, Y.R. Lee, Biosynthesis of Fe, Pd, and Fe–Pd bimetallic nanoparticles and their application as recyclable catalysts for [3 + 2] cycloaddition reaction: a comparative approach, *Catal. Sci. Technol.* 5 (2015) 2612–2621, <https://doi.org/10.1039/C5CY00099H>.
- [42] X. Li, W. Zhang, Sequestration of metal cations with zero valent iron nanoparticles: A study with high resolution X-ray photoelectron spectroscopy (HR-XPS), *J. Phys. Chem. C* 111 (2007) 6939–6946, <https://doi.org/10.1021/jp0702189>.
- [43] M.S. Tiwari, G.D. Yadav, F.T.T. Ng, Selective hydrogenation of 3,4-dimethoxybenzophenone in liquid phase over Pd/C catalyst in a slurry reactor, *Can. J. Chem. Eng.* 92 (2014) 2157–2165, <https://doi.org/10.1002/cjce.22073>.
- [44] N.S. Babu, N. Lingaiah, J.V. Kumar, P.S.S. Prasad, Studies on alumina supported Pd – Fe bimetallic catalysts prepared by deposition – precipitation method for hydrodechlorination of chlorobenzene, *Appl. Catal. A Gen.* 367 (2009) 70–76, <https://doi.org/10.1016/j.apcata.2009.07.031>.
- [45] S. Nishimura, *Handbook of Heterogeneous Catalytic Hydrogenation for Organic Synthesis*, Wiley, New York, 2001.
- [46] J. Molleti, M.S. Tiwari, G.D. Yadav, Novel synthesis of Ru/OMS catalyst by solvent-free method: Selective hydrogenation of levulinic acid to  $\gamma$ -valerolactone in aqueous medium and kinetic modelling, *Chem. Eng. J.* 334 (2018) 2488–2499, <https://doi.org/10.1016/j.cej.2017.11.125>.